Vibrational excitation of methane by positron impact: Computed quantum dynamics and sensitivity tests

Tamio Nishimura* and Franco A. Gianturco[†]

Department of Chemistry, The University of Rome, Città Universitaria, 00185 Rome, Italy
(Received 27 December 2001; published 3 June 2002)

We report the quantum dynamical close-coupling equations relevant for vibrationally inelastic processes in low-energy collisions between a beam of positrons and the CH_4 molecule in the gas phase. The interaction potential is described in detail and we report also our numerical technique for solving the scattering equations. The cross sections are obtained for the excitations of all the modes of the title molecule and are compared both with simpler computational approximations and with the recent experiments for the two distinct energy regions that correspond to the combined symmetric and antisymmetric stretching modes and to twisting and scissoring modes, respectively. Our calculations reproduce well the shape and the values of the experimental findings and give useful insights into the microscopic dynamics for molecular excitation processes activated by low-energy positron scattering.

PACS number(s): 34.10.+x, 34.90.+q

I. INTRODUCTION

Vibrational excitation of molecules by electron (e^-) or positron (e^+) impact is one of the elementary processes of interest in diverse fields such as gaseous electronics, plasma chemistry, planetary science, and astrophysics [1,2]. The general picture usually employed to describe such processes qualitatively shows the incident projectile as distorting the electron cloud of the target molecule, which in turn exerts a deforming force on the molecular nuclei, causing displacement of the nuclear configuration from its equilibrium. In the end, the projectile loses part, or all, of its energy into a vibrationally excited state of the molecule. As a continuation of our work on the vibrational excitation of polyatomic molecules in the gas phase, by positron [3,4] and by electron impact [5,6], we report in this paper a detailed study of computed cross sections for vibrationally inelastic scattering of positrons from methane (CH_4). The use of a positron as a projectile, instead of an electron, adds some interesting phenomena to the collision system considered. Needless to say, an incident positron is distinguishable from all the bound electrons of the molecular target so there is no effect from electron exchange contributions that need instead to be considered in the case of electron-molecule collisions. Furthermore, a positron has the possibility of picking off one of the electrons of the target, thereby forming a positronium (Ps) atom, provided that the collision energy is above the threshold for the Ps formation energy, which is 5.8 eV for the e^+-CH_4 system.

The CH_4 molecule belongs to the T_d point group and has four types of normal modes that describe its lower-lying vibrations, i.e., the symmetric stretching (ν_1), the twisting (ν_2), the antisymmetric stretching (ν_3), and the scissoring

(ν_4) modes (see Fig. 1 and Tables I and II). Thus, if the polyatomic molecule is considered as having little vibrational energy in the gas sample, the excitation processes could be treated as occurring separately for the different normal modes that carry different fundamental frequencies and belong to different symmetries. It is therefore interesting to try to understand, within this somewhat simplified picture, how the separate excitation for each normal mode depends
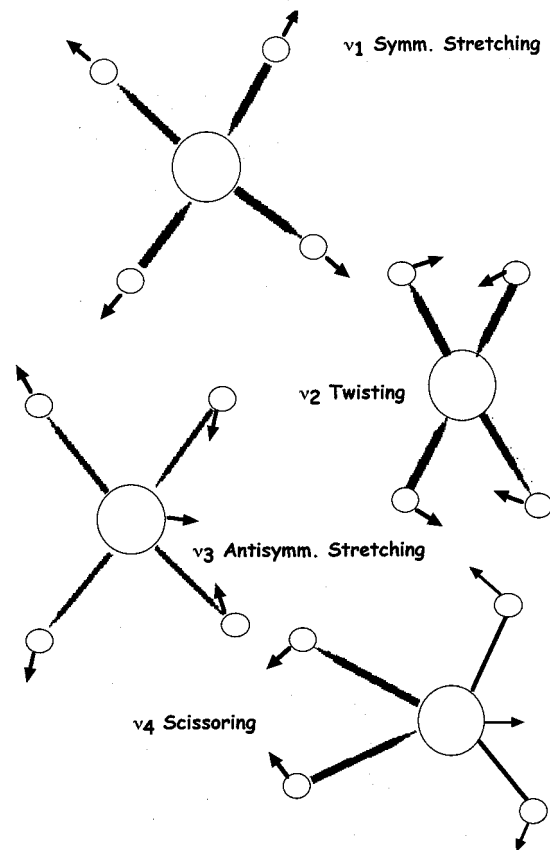

FIG. 1. Pictorial representation of the four normal modes for a molecule that belongs to the T_d point group.

---

*Permanent address: 2-11-32, Kawagishi-kami Okaya, Nagano 3940048, Japan.

[†]Author to whom correspondence should be addressed. FAX: +39-06-49913305. Email address: fa.gianturco@caspur.it

TABLE I. Vibrational modes of CH_4.

Mode	Frequency (eV)		Symmetry	Activity
	Expt.[a]	Calc.		
ν_1 (symm. stretch)	0.362	0.390	A_1 (T_d)	Raman (R)
ν_2 (twisting)	0.190	0.207	E (D_2)	Raman (R)
ν_3 (antisymm. stretch)	0.374	0.402	T_2 (C_s)	Infrared (IR)
ν_4 (scissoring)	0.162	0.180	T_2 (C_{2v})	Infrared (IR)

[a]The recommended values based on experiments [32].

on the feature of the specific mode involved without as yet considering the mixing within the modes that are expected to physically occur when "hotter" molecular targets are examined. In particular, since the ν_3 and the ν_4 modes are infrared (IR) active, a long-range interaction due to an induced dipole moment is expected to be effective for them, as opposed to the ν_1 and the ν_2 modes that are instead Raman (R) active and involve no induced dipole contributions.

Total cross sections (TCSs) for many types of atoms and molecules have been reported in the literature (see [7,8] and references quoted therein), due to the development of better collimated positron beams [9], while only recently the relative differential cross sections of elastic processes for CH_4 have been reported over a large range of scattering angles (30°–135°) [9]. In that case, however, the data still correspond to quasielastic (elastic scattering plus rotational and vibrational excitations) cross sections because of the fairly large energy spread of their positron beams with a full width at half maximum (FWHM) of about 2 eV. The development of a novel experimental technique involving a magnetized beam of cold positrons [10] allowed measurements of absolute vibrationally inelastic cross sections for CO, CO_2, and H_2 [11] and also for CH_4 [12]. The data have been collected for the first time at energies as low as 0.5 and up to several eV with a greatly improved FWHM value of 18 meV. These experiments have thus stimulated the interest of theoreticians and spurred the formulation of computational methods that could provide explanation as to how the phenomenon is occurring at the nanoscopic level. In the case of H_2, we have actually calculated vibrational excitation cross sections [4] that reproduce well the experimental findings [4,11], and the same occurs for the case of the CO molecule [11,13]. As for CH_4, due to the higher resolution required, the excitation

processes of the ν_1 and the ν_3 modes, as well as those of the ν_2 and the ν_4 modes, cannot be completely resolved by current measurements. Because of these difficulties, therefore, the experimental data need even more to be supplemented by theoretical analysis, to better understand the complete picture of the vibrational excitation dynamics triggered by positron projectiles.

The present calculation is based on the fixed nuclear orientation (i.e., the rotationally sudden) approximation [14]. The vibrational transition is treated within a closed-coupling method discussed in detail in the following section. It basically extends to the polyatomic targets given in the earlier proposals for diatomic molecules [15]. In a preliminary study [16], we have presented and discussed the computed cross sections for the collisional excitation of the ν_1 and the ν_3 modes, and we showed there that our calculations reproduced well the shape of experimental findings [12]. In this paper, the calculations are extended to all the normal modes and various theoretical features, which come into play at threshold energies for the inelastic cross sections, are examined. They allow us to get a better physical insight into the dynamics of the excitation process.

The details of the present theory and of the simplifications used to analyze threshold effects are described in Sec. II, where our numerical techniques are also presented extensively. In Sec. III we report on the final cross sections and discuss their behavior with reference to various experiments and to other available calculations. We give our present conclusions in Sec. IV. Atomic units (a.u.) are used throughout the present analysis unless otherwise stated.

II. THE THEORETICAL APPROACH

Since the details of the present theory have been given before [16,17], we provide the reader only a brief reminder

TABLE II. Range of internal coordinates for the four vibrational normal modes of CH_4. r_i is the bond length (Å) of C-H_i, θ_{ij} is the molecular angle (deg) of $\angle H_iCH_j$, β_{AB} is the angle (deg) between the planes of $\angle H_1CH_3$ and $\angle H_2CH_4$. Vibrational displacements for the normal coordinates are given as ΔR_s [(amu)$^{1/2}$ Å] $= \pm 1$.

	r_1	r_2	r_3	r_4	θ_{13}	θ_{24}	β_{AB}
$R_{eq.}$	1.082	1.082	1.082	1.082	109.47	109.47	90.0
ν_1	±0.502	±0.502	±0.502	±0.502			
ν_2							±58.18
ν_3	±0.557	∓0.544	±0.540	∓0.544			
ν_4					±51.46	∓51.46	

of them. In order to obtain vibrational excitation cross sections we need to solve the Schrödinger equation of the composite system at a fixed value of the total energy E. Here the total Hamiltonian is given by

$$\hat{H} = \hat{H}_{\text{mol.}} + \hat{K} + \hat{V}, \tag{1}$$

where $\hat{H}_{\text{mol.}}$, $\hat{K}$, and $\hat{V}$ represent the operators of the molecular Hamiltonian, of the kinetic energy for the scattered positron, and of the interaction between the incident positron and the target molecule, respectively. The $\hat{H}_{\text{mol.}}$ of this study only consists of the rotational and vibrational parts of the more complicated, full molecular electronuclear Hamiltonian. Hence, we include no effect from possible electronic excitations or from other reactive and breakup processes. In other words, we assume that during the scattering the molecular electronic wave function is always that of its neutral ground electronic state A_1. It should also be noted here that no Ps formation channel is considered throughout the present calculations as it seems to be fairly negligible at the energies below the Ps formation threshold of the collision system considered.

We also assume that the orientation of the target molecule is fixed during the collision, i.e., we invoke what goes under the name of the rotationally sudden approximation, since the molecular rotation is usually slower when compared with the velocity of the projectile at the energies we are considering. This is also called the fixed-nuclear orientation (FNO) approximation [14], and corresponds to ignoring the rotational Hamiltonian in $\hat{H}_{\text{mol.}}$ of Eq. (1). Then, the total wave function could be expanded as follows:

$$\Psi(\mathbf{r}_p|\mathbf{R}) = r_p^{-1} \sum_{l\nu n} u_{l\nu n}(r_p) X_{l\nu}(\hat{\mathbf{r}}_p) \chi_n(\mathbf{R}). \tag{2}$$

Here, χ_n is the vibrational wave function of the molecule with its quantum number $n \equiv (n_1, n_2, \ldots, n_s, \ldots, n_T)$, where T represents the total number of normal vibrational modes of the target. The variables $\mathbf{R}$ and $\mathbf{r}_p$ denote the nuclear geometry and the position vector of the positron from the center of mass of the target, respectively. The unknown $u_{l\nu n}$ functions describe the radial coefficients of the positron wave function and the $X_{l\nu}$ are the symmetry-adapted angular basis functions introduced earlier by us [18]. The symbol ν in Eq. (2) globally stands for the indices specifying the irreducible representation and those distinguishing its degenerate members.

After substituting Eq. (2) into the Schrödinger equation of the total system (under the FNO approximation) we obtain a set of full close-coupling equations for $u_{l\nu n}$ (τ_p) that now include vibrational channels. These are called the body-fixed vibrational close-coupling (BF-VCC) equations [4,16],

$$\left\{ \frac{d^2}{dr_p^2} - \frac{l(l+1)}{r_p^2} + k_n^2 \right\} u_{l\nu n}(r_p)$$

$$= 2 \sum_{l'\nu'n'} \langle l\nu n|V|l'\nu'n' \rangle u_{l'\nu'n'}(r_p), \tag{3}$$

where k_n is written as

$$k_n^2 = 2(E - E_n^{\text{vib}}), \tag{4}$$

with $E_n^{\text{vib.}}$ being the energy of the specific molecular vibration we are considering. Any of the elements of the interaction matrix in Eq. (3) is given by

$$\langle l\nu n|V|l'\nu'n' \rangle$$

$$= \sum_{l_0\nu_0} \langle n|V_{l_0\nu_0}|n' \rangle \int d\hat{\mathbf{r}}_p X_{l\nu}(\hat{\mathbf{r}}_p)^* X_{l_0\nu_0}(\hat{\mathbf{r}}_p) X_{l'\nu'}(\hat{\mathbf{r}}_p), \tag{5}$$

where

$$\langle n|V_{l_0\nu_0}|n' \rangle = \int d\mathbf{R} \{\chi_n(\mathbf{R})\}^* V_{l_0\nu_0}(r_p|\mathbf{R}) \{\chi_{n'}(\mathbf{R})\}. \tag{6}$$

When solving Eq. (3) under the usual boundary conditions, the asymptotic form of $u_{l'\nu'n'}^{l\nu n}$ is represented by a sum containing the incident plane wave of the projectile and the outgoing spherical wave. Thus, the final integral cross section for the vibrationally inelastic scattering is given by

$$Q(n \to n') = \frac{\pi}{k_n} \sum_{l\nu} \sum_{l'\nu'} |T_{l'\nu'n'}^{l\nu n}|^2, \tag{7}$$

where $T_{l'\nu'n'}^{l\nu n}$ is the T-matrix element produced by the boundary matching [16].

The interaction between the impinging positron and the molecular target is represented here in the form of a local potential. Thus, it is described by the sum of the repulsive electrostatic (V^{st}) and the attractive positron correlation–polarization (V^{pcp}) terms. Possible cancellations in specific regions of space could occur between the two potential terms because they have opposite signs, a feature specific to positron dynamics that makes the resulting cross section to be very sensitive to the particular form of V^{pcp} which is being employed in the calculations. To obtain the V^{pcp} in the shorter range of $\mathbf{r}_p$, use is made of a simple parameter-free model potential (V^{corr}) based on an electron-positron correlation energy (ε^{e-p}) suggested by Boronski and Nieminen [19] in the framework of a homogeneous electron gas [20],

$$V^{\text{corr}}(\mathbf{r}_p|\mathbf{R}) = \frac{d}{d\rho} \{\rho(\mathbf{r}_p|\mathbf{R}) \varepsilon^{e-p}[\rho(\mathbf{r}_p|\mathbf{R})]\}, \tag{8}$$

where ρ denotes the undistorted electron density of the target correctly obtained from many-body calculations. In our implementation of this model, the short-range V^{corr} is connected smoothly with the asymptotic form (V^{pol}) of its spherical component [21],

$$V^{\text{pol}}(\mathbf{r}_p|\mathbf{R}) \underset{r_p \to \infty}{\sim} -\frac{\alpha_0(\mathbf{R})}{2\mathbf{r}_p^4}. \tag{9}$$

Here, α_0 is the target polarizability of the spherical component denoting the dipole term.

TABLE III. Computational details of the two-state BF-VCC calculation.

Normal mode	Point group	$l_{0,\max}$	$l_{\max}$	Maximum number of coupled channels
ν_1	T_d	24	12	$A_1 = 22$, $A_2 = 8$, $E = 28$, $T_1 = 36$, $T_2 = 48$
ν_2	D_2	28	14	$A = 114$, $B_1 = 112$, $B_2 = 112$, $B_3 = 112$
ν_3	C_s	24	12	$A = 182$, $B = 156$
ν_4	C_{2v}	24	12	$A_1 = 98$, $A_2 = 72$, $B_1 = 84$, $B_2 = 84$

In order to obtain a better insight into the dynamical features of vibrational excitation processes we expand $V_{l_0 \nu_0}$ of Eq. (6) around the equilibrium geometry of the target $R_{\mathrm{eq.}}$ [14,22],

$$V_{l_0 \nu_0}(r_p | \mathbf{R}) = V_{l_0 \nu_0}(r_p | R_{\mathrm{eq.}})$$

$$+ \sum_s \left\{ \frac{\partial V_{l_0 \nu_0}(r_p | R_s)}{\partial R_s} \right\}_{R_s = R_{\mathrm{eq.}}} (R_s - R_{\mathrm{eq.}})$$

$$+ \text{higher-order terms.} \tag{10}$$

Thus, whenever we wish to consider a transition to a low-lying excited state close to the initial state, the higher-order terms on the right-hand side of Eq. (10) are expected to give small contributions to the total vibrational matrix element and therefore could be ignored. In the present case, the matrix element of Eq. (6) could also be approximately evaluated as follows:

$$\langle n | V_{l_0 \nu_0} | n' \rangle = \langle n | V_{l_0 \nu_0}^{\mathrm{st}} + V_{l_0 \nu_0}^{\mathrm{pcp}} | n' \rangle \simeq V_{l_0 \nu_0}^{\mathrm{st}}(r_p | R_{\mathrm{eq.}}) \delta_{nn'}$$

$$+ \sum_s \left\{ \frac{\partial V_{l_0 \nu_0}^{\mathrm{st}}(r_p | R_s)}{\partial R_s} \right\}_{R_s = R_{\mathrm{eq.}}} \langle n | R_s - R_{\mathrm{eq.}} | n' \rangle$$

$$+ V^{\mathrm{pcp}} \text{ contributions,} \tag{11}$$

where

$$\langle n | R_s - R_{\mathrm{eq.}} | n' \rangle = \left\{ \left[\sqrt{(n_s+1)/2} \, \right] \delta_{n_s', n_s+1} \right.$$

$$\left. + (\sqrt{n_s/2}) \delta_{n_s', n_s-1} \right\} \prod_{t(\neq s)} \delta_{n_t', n_t}, \tag{12}$$

if we assume the molecular vibration to be harmonic [23]. The superscript "st" in Eq. (11) describes the global contributions of the electrostatic potential through its multipole moments, and we omit for the moment to write down explicitly the contributions from the V^{pcp} interaction. When the incident projectile is sufficiently far from the target molecule, the term of $V_{l_0 \nu_0}^{\mathrm{st}}$ is given by its leading multipoles as [14]

$$V_{l_0 \nu_0}^{\mathrm{st}}(r_p | \mathbf{R}) \underset{r_p \to \infty}{\sim} -\left(\frac{4\pi}{2l_0+1} \right)^{1/2} \frac{M_{\nu_0}^{l_0}(\mathbf{R})}{r_p^{l_0+1}}, \tag{13}$$

where $M_{\nu_0}^{l_0}$ involves all the contributing electric multipole moments of the molecule. With the use of the relation (13) we can, therefore, examine the accuracy of this approximate picture through the evaluation of the leading contributing moments to the above matrix element. This analysis will be carried out below, after describing in detail our numerical treatment.

A. Numerical details

The target wave function of the electronic ground state for CH_4 was calculated at the SCF (self-consistent field) level using our familiar single-center expansion method [24] applied to a multicenter Gaussian-type orbitals (GTOs), and the basis set employed was provided by the GAUSSIAN 98 package [25]. We have chosen the GTO basis sets of D95* type that involves 46 primitive Gaussians contracted to 24 basis functions $((9s5p1d)/[4s2p1d]$ for carbon, and $(4s)/[2s]$ for hydrogen). It gives a total energy of -40.2006 a.u. at $R_{\mathrm{eq.}}$, as reported in Table II. The terms of the multipolar expansion of the interaction potential in Eq. (5) were retained up to $l_{0,\max}$, and the scattered wave function of the positron in Eq. (2) was expanded, with the inclusion of the lowest two vibrational states $n=0$ and $n=1$, up to $l_{\max}$, which yielded K-matrix elements converged within 1%. For the specific information of all the required parameters and properties for each of the vibrations we study in the present work, see Table III. In order to solve the close-coupling equations by means of standard Green's function techniques, Eq. (3) is rewritten as an integral equation (a Volterra equation: for details, see Ref. [26]). In the case of the ν_1 mode that belongs to the A_1 irreducible representation, by fixing the molecular symmetry to be that of the T_d point group, the range of bond length of C-H was taken to vary from 0.87 to 1.6 Å in order to sufficiently take into account the effects of the nuclear displacements from $R_{\mathrm{eq.}}$ for the lowest four vibrational levels. As for the other modes, the vibrational normal coordinates R_s were taken to vary in the range of values given in Table II. For the asymptotic part of the V^{pcp}, i.e., V^{pol}, we first obtain the values of α_0 from a very large basis set [27] that consists of $(24s8p4d3f2g1h)/[6s5p4d3f2g1h]$ for carbon and $(8s4p3d2f1g)/[5s4p3d2f1g]$ for hydrogen and gives the α_0 of 15.45 a.u. at $R_{\mathrm{eq.}}$. (The computed α_0 as a function of R_s, e.g., for the ν_1 mode is given in Fig. 2 and is labeled 2.) We further normalize our calculations to the experimental value of α_0 (17.54 a.u.) which is known for $R_{\mathrm{eq.}}$, and the result is shown in Fig. 2 (curve no. 1).
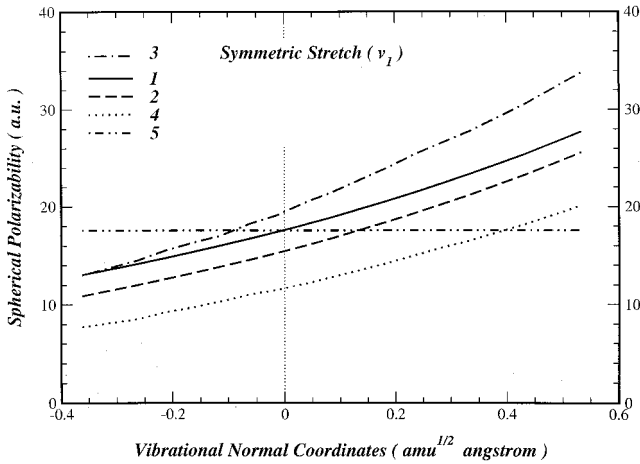
FIG. 2. Five sets of computed dipole polarizabilities of the spherical component for the ν_1 mode of the CH_4 molecule. See text for details.

B. The asymptotic couplings

In order to analyze in more detail the leading terms that contribute to the approximate expression of Eq. (10) described in Eq. (11), we need to evaluate the derivative of the transition dipole moment (TDM) with respect to the R_s at $R_{eq.}$ i.e., $\partial\mu_{\nu_0}(R_s)/\partial R_s|_{R_s=R_{eq.}}$. We first obtained the TDM (μ_{ν_0}), according to Eq. (13), using the static contributions $V^{st}_{l_0\nu_0}$ for the A_1 irreducible representation with $(l_0,\nu_0) = (1,1)$ for ν_3 and $(1,0)$ for ν_4, computing them as a function of R_s (see Fig. 3). Then, we obtained the derivative by means of a straightforward numerical differentiation by the following formula:
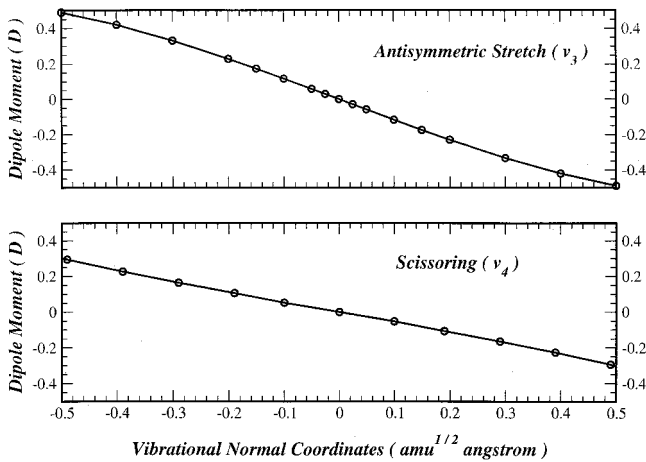
FIG. 3. Calculated induced dipole moments for the antisymmetric stretching mode (ν_3) (top panel) and those for the ν_4 (lower panel) of CH_4 as a function of the vibrational normal coordinates.

TABLE IV. Derivatives of the induced dipole moments for the ν_3 and ν_4 modes.

Derivative (D amu$^{-1/2}$ Å^{-1})	Present[a]	Experiment[b]	Experiment[c]
$\partial\mu_1/\partial R_3\vert_{R_3=R_{eq.}}$	1.18	0.719	1.65
$\partial\mu_0/\partial R_4\vert_{R_4=R_{eq.}}$	0.582	0.501	0.815

[a]From the present calculations without scaling.
[b]Derived from experimental IR intensities as given in Ref. [29].
[c]Estimated from the measured inelastic cross sections of Ref. [12].

$$\left\{\frac{\partial\mu_{\nu_0}(R_s)}{\partial R_s}\right\}_{R_s=R_{eq.}}$$

$$=\left\{\frac{\mu_{\nu_0}(R_s+\Delta R_s)-\mu_{\nu_0}(R_s-\Delta R_s)}{2\Delta R_s}\right\}_{R_s=R_{eq.}}. \tag{14}$$

We should also remember that the TDM derivative is related to the IR absorption intensity A_s and can be obtained from experimental data [14,28]

$$A_s(n\rightarrow n')\ \ (\text{km}\,\text{mol}^{-1})$$

$$=16.192\omega_s\ (\text{cm}^{-1})\sum_{\nu_0}\ |\langle n|M^{l_0=1}_{\nu_0}|n'\rangle^s|^2\ \ (\text{a.u.}), \tag{15}$$

where

$$|\langle n|M^{l_0=1}_{\nu_0}|n'\rangle^s|^2\ \ (\text{a.u.})$$

$$=\frac{2.6095g_s}{\omega_s\ (\text{cm}^{-1})}\left[\left\{\frac{\partial\mu_{\nu_0}(R_s)}{\partial R_s}\right\}_{R_s=R_{eq.}}[D\ (\text{amu})^{-1/2}A^{-1}]\right]^2 \tag{16}$$

with g_s and ω_s being the degeneracy of the mode and the corresponding IR frequency respectively. Hence, we can also derive estimates for the above TDM matrix elements by making use of the measured IR intensity. Table IV shows the computed and measured values of $\partial\mu_{\nu_0}(R_s)/\partial R_s|_{R_s=R_{eq.}}$ for the ν_3 and the ν_4 modes, for the $\Delta n=1$ transitions. As experimental values we employed the data given in Ref. [29]. When we compare with experiments the present calculations obtained within a fairly simple SCF description of the molecular electronic density, we find that our results give a reasonably good value of $\partial\mu_{\nu_0}/\partial R_s|_{R_{eq.}}$ for the ν_4 mode, while we obtain a larger estimate for the ν_3 mode. Following

TABLE V. Computed derivatives of the spherical polarizability.

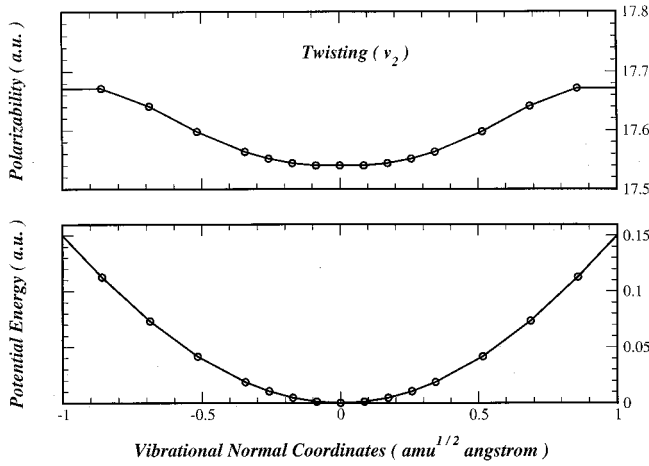| Derivative (amu$^{-1/2}$ Å^2)	ν_1	ν_2	ν_3	ν_4
$\partial\alpha_0/\partial R_3\vert_{R=R_{eq.}}$	2.18	0.00	8.88×10^{-3}	0.00

FIG. 4. Calculated dipole polarizabilities of the spherical component (top panel) and the corresponding potential energy curve (lower panel) of CH_4 as a function of the vibrational normal coordinates for the twisting mode (ν_2).

Eq. (14) we also estimate (see Table V) the derivative of the spherical polarizability $\partial\alpha_0/\partial R_s|_{R_s=R_{eq.}}$ that is related to the long-range part of the polarization potential gradient $\partial V^{pol}/\partial R_s|_{R_s=R_{eq.}}$. Since the α_0 is represented as

$$\alpha_0(\mathbf{R}) = \tfrac{1}{3}\{\alpha_{xx}(\mathbf{R}) + \alpha_{yy}(\mathbf{R}) + \alpha_{zz}(\mathbf{R})\}, \qquad (17)$$

when we consider the symmetric and almost symmetric features of the present normal modes (with the exception of the ν_1) with respect to $R_{eq.}$, one quickly discovers from Figs. 2, 4, and 5 for the ν_1, ν_2, and ν_4 modes (see Ref. [16] for the ν_3 mode), that the values of $\partial\alpha_0/\partial R_s|_{R_s=R_{eq.}}$ for ν_2 and ν_4 are zero while that for ν_3 is much smaller than that for the ν_1 mode. The latter vibration therefore indicates the behavior of α_0 as a function of R_s to be antisymmetric, as shown in Fig. 2. We shall show below that all these different features of the gradient-driven transition matrix elements for the dominant terms of the coupling potentials play an important role for
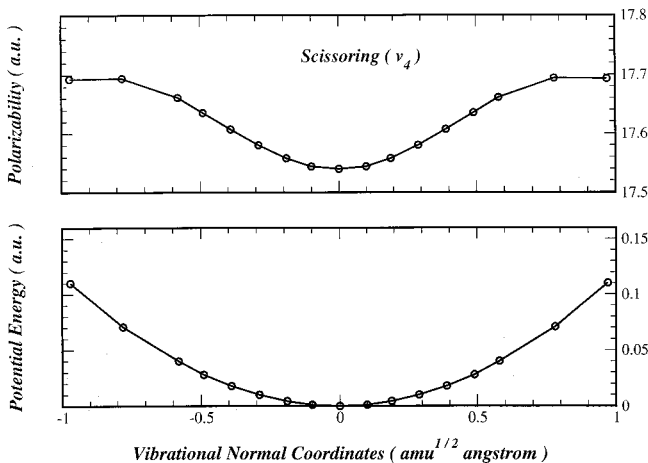

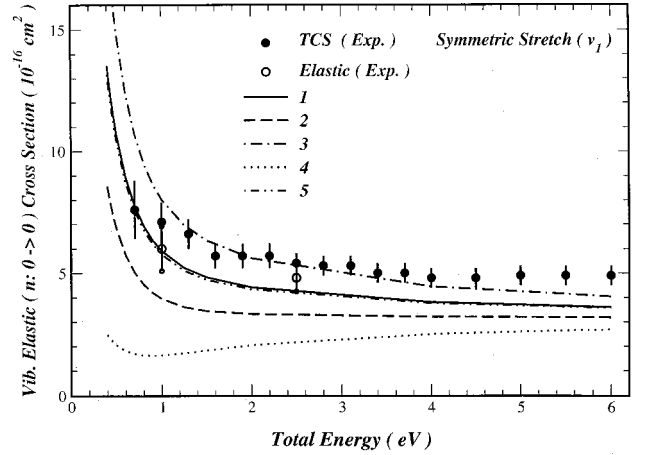FIG. 5. Same as in Fig. 4 but for the scissoring mode (ν_4).

FIG. 6. Computed cross sections, obtained from the five sets of estimated polarizabilities in Fig. 2, for the vibrationally elastic scattering ($0\rightarrow0$) in the ν_1 mode, using the two state BF-VCC method. The present cross sections are compared with the experimental elastic cross sections (open circles) and with the total ones [30] (full circles). The former quantity is derived by subtracting the contribution of the vibrational excitation cross sections [12] from the total [30].

the vibrational excitation cross sections analyzed in the present work, especially in the very low energy region near each vibrational threshold.

III. DISCUSSION OF PRESENT RESULTS

If we begin with the ν_1 mode, which belongs to the T_d point group, the leading terms of the anisotropic interaction potential in Eq. (5), i.e., $V_{l_0\nu_0}$ with $(l_0,\nu_0)\neq(0,A_1)$, give a rather small contribution to the final sum of all potential terms. The spherical component of the $(l_0,\nu_0)=(0,A_1)$ has its repulsive V^{st} potential dominant at small r_p while, as r_p increases, the repulsive effects turn into the attractive contributions from the V^{pol} and further go through a point where the relationship $V^{st}+V^{pcp}=0$ is satisfied. In the asymptotic region of r_p, the potential is almost exclusively described by the attractive spherical V^{pol} represented by Eq. (9). (For more details on the behavior of the spherical component of the potential at $R_{eq.}$, see also Fig. 11 in Ref. [7]). From the above features of the potential, therefore, the collision dynamics in the ν_1 mode is the simplest one for which we can visualize the effects from $\partial\alpha_0/\partial R_s|_{R_s=R_{eq.}}$ on the final vibrational excitation cross sections. We, therefore, generated five different sets of α_0 as a function of R_s ($s=1$) for the ν_1 mode and report them in Fig. 2. We obtain the sets numbered 1 and 2 as described before in Sec. II A, while we artificially produced those labeled as 3 and 4 to yield larger and smaller gradient values around $R_{eq.}$. For the set labeled 5 the α_0 was fixed at its experimental equilibrium value throughout the examined range of R_s. In the case of vibrationally elastic scattering, ($n:0\rightarrow0$), as the α_0 is large around $R_{eq.}$, the computed cross section also turns out to be fairly large (see Fig. 6): the model cross sections computed from all the choices of Fig. 2 shows that the elastic data numbered 1 and
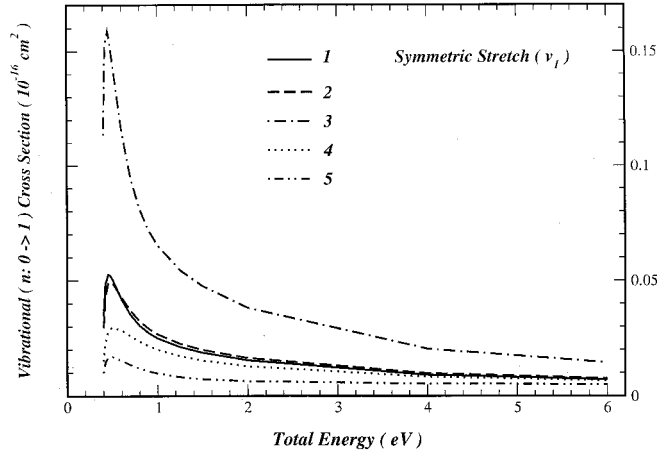
FIG. 7. Same as in Fig. 6 but for the vibrationally inelastic process ($0 \to 1$) in the ν_1 mode. Calculations are done via the BF-VCC method including two vibrational channels, $n=0$ and 1.

FIG. 8. Calculated dipole polarizability as a function of the vibrational normal coordinates for the ν_4 mode (top panel) and the corresponding vibrationally inelastic cross sections ($0 \to 1$) by the BF-VCC as a function of the total energy (lower panel). The solid line refers to the values of α_0 normalized to the experimental value at the equilibrium geometry, after computing the α_0 as a function of the normal coordinates. The circles were obtained by using an artificial value of α_0 constrained to be the measured value at the equilibrium geometry.

5, which employ the experimental value of α_0 at $R_{eq.}$, turn out to reproduce reasonably well the experimental elastic cross sections. The latter were derived approximately from the measured vibrational excitation data [12] by subtracting them from the TCSs given also by experiments [30].

On the other hand, when we analyze in a similar way the inelastic process, the ($n:0 \to 1$) excitation, as expected from the form of the coupling matrix element given by Eq. (11), we find that also the $\partial\alpha_0/\partial R_s|_{R_s=R_{eq.}}$ plays a crucial role. From Figs. 2 and 7 we see that, as the gradient around the $R_{eq.}$ gets larger, the ensuing cross section becomes larger. It should be noted that the cross sections labeled 1 and 2 in Fig. 7 are very close to each other since the set of the model α_0 labeled 1 in Fig. 2 is obtained by a parallel shift of that labeled 2 over the whole range of R_s, hence there is no gradient change in going from set 1 to set 2. The BF-VCC cross sections for the ν_1 mode discussed below will then be obtained by employing the set of α_0 values labeled as 1 in Fig. 2.

In the case of the other three modes, the contribution of α_0 to the vibrational excitation matrix elements is rather small for the ν_3 and null for the ν_2 and ν_4 because, as shown in Table V, the value of $\partial\alpha_0/\partial R_s|_{R_s=R_{eq.}}$ for these modes is either zero or very small, and almost no contribution comes from this quantity to the interaction matrix element of Eq. (11). The data of Fig. 8 clearly show, in fact, that the effect of α_0 on the inelastic process is highly negligible for the ν_4 mode.

The vibrationally inelastic cross sections of the ν_2^z, ν_3^z, and ν_4^z (z component only) modes are reported in Figs. 9, 10, and 11, respectively. We show there different aspects of the calculations which we have carried out in the present work. (For the ν_1 mode, see Fig. 4 in Ref. [16].) In these figures, the open circles denote the more simple calculations associated with the adiabatic nuclear vibration (ANV) approximation described before [5,6]. No direct dynamical coupling is active during the scattering process and the transition T matrix is computed by a simple adiabatic convolution over the
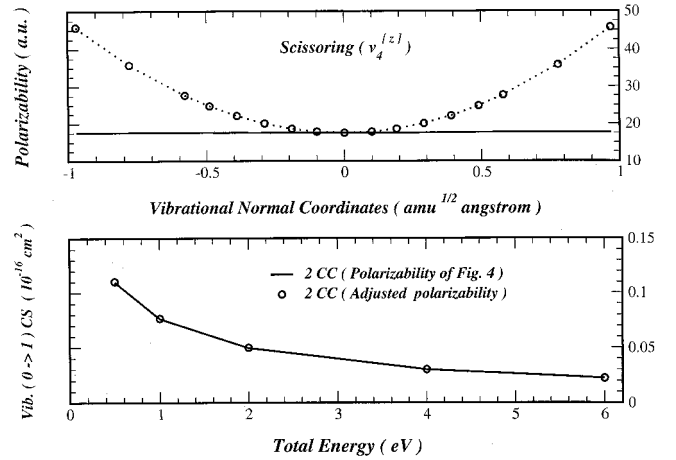
initial and the final vibrational wave functions for each specific mode of the target,

$$T^{l\nu n}_{l'\nu'n'} = \int d\mathbf{R}\{\chi_{n'}(\mathbf{R})\}^* T^{l\nu}_{l'\nu'}(\mathbf{R})\{\chi_n(\mathbf{R})\}. \quad (18)$$

Only the first vibrational threshold is presented for each of the modes. The solid lines show the BF-VCC results that already reached convergence when the first two open channels ($n=0$ and 1) were considered. The inclusion of higher, closed channels essentially leaves the final cross sections unchanged except for energy regions in the very vicinity of vibrational excitation thresholds [31]. We, therefore, report here only the results with two dynamically coupled vibra-
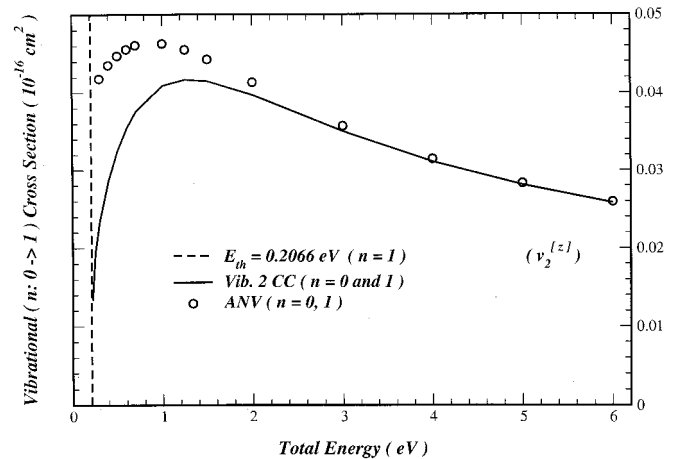

FIG. 9. Vibrational excitation cross sections for the ν_2 mode. The present cross section via the BF-VCC approach (solid curve) is compared with that obtained by the ANV method (open circles).
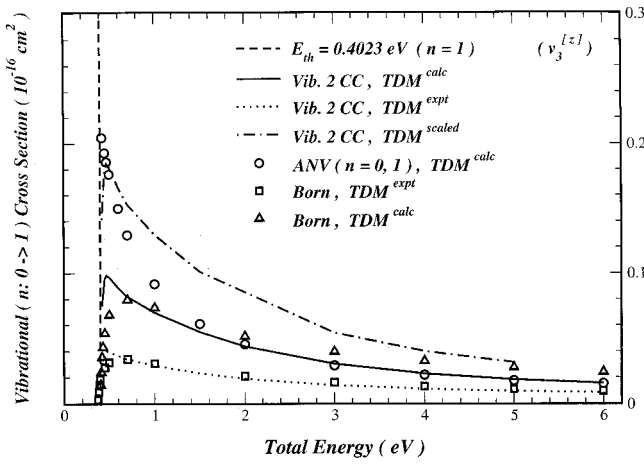
FIG. 10. Same as in Fig. 9 but for the ν_3 mode. The cross section via the BF-VCC (solid curve) is also compared with that obtained with the dipole Born approximation [14]. The latter results are based on the calculated quantities for the vibrational frequency and the dipole derivative (triangles) and on their corresponding experimental values [29,32] (squares). The dotted curve reports the BF-VCC results obtained by adjusting the computed dipole derivative component by a factor of 0.609 to match the IR experimental value [29]. Moreover, the chain curve reports our calculations obtained by scaling the computed dipole derivative by the factor of 1.4.

tional channels. This feature is a clear indication of the rather weak coupling that exists between the motion of the molecular nuclei and that of the positron projectile during the scattering process. The comparison between the exact (at least within our modeling of the interaction) treatment of the vibrational dynamics, i.e., the BF-VCC method, and the more approximate ANV results is really very satisfactory with the obvious exclusion of the threshold region where the physical cross sections should go to zero (as the BF-VCC calculations do) while the ANV data do not. Although the closeness between the two methods is very similar for all modes, small differences become already noticeable at around 2 eV of total energy (i.e., well above the threshold) in the case of the ν_2^z
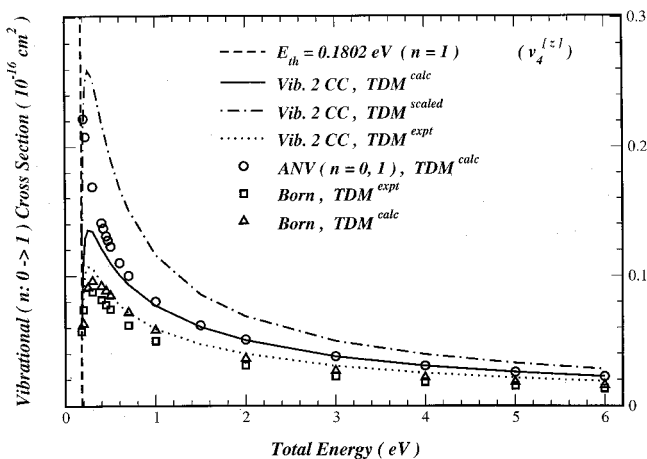

FIG. 11. Same as in Fig. 10 but for the ν_4 mode.

and the ν_3^z modes. This means that the rather weak coupling between the positron and the molecular nuclei does not really require one to include corrections from the projectile kinetic energy term during the scattering process and therefore, away from thresholds, choosing a simpler, asymptotic-type wave vector is already sufficient. This is a very interesting conclusion that bears great significance for carrying out further calculations that may involve more complex polyatomic targets. We have analyzed before [6] the effects of introducing a kinematic scaling of the ANV cross sections to make them behave correctly at threshold. However, because of our present interest in threshold effects, we did not repeat here this correction that was shown to incorrectly describe any threshold structure [6].

In the case of the ν_3^z and ν_4^z modes we also report in Figs. 10 and 11 the Born cross sections obtained by employing only the coupling from the TDM effects [14],

$$Q_s^{\text{Born,dip}}(n \to n') = \frac{8\pi}{3k_n^2} \ln \left| \frac{k_n + k_{n'}}{k_n - k_{n'}} \right| \sum_{\nu_0} |\langle n | M_{\nu_0}^{l_0=1} | n' \rangle^s|^2$$

(19)

with $g_s = 1$ of Eq. (16) for the z component of the two modes. In the present study, we obtained the cross sections by substituting into Eq. (19), through Eq. (16), values of the $\partial \mu_{\nu_0}/\partial R_s|_{R_s = R_{\text{eq.}}}$ and of the frequency for the two modes given in Tables I and IV obtained respectively by either the present SCF calculations or from the IR intensity experiments [29,32]. In the case of ν_3^z, the Born cross section obtained via our computed TDM (triangles) is larger than that obtained by using the experimental values (squares), while for ν_4^z (see Fig. 11), the two sets of cross sections are much closer to each other. These results suggest that the magnitude of $\partial \mu_{\nu_0}/\partial R_s|_{R_s = R_{\text{eq.}}}$ markedly controls the strength of the peaks appearing in the cross sections for the ν_3^z and ν_4^z modes just above the threshold of $n=1$, as we shall further discuss below.

To see the effects of the TDM on the cross sections, we artificially adjusted the computed $V_{l_0 \nu_0}^{\text{st}}$ dipole component of $l_0 = 1$ by scaling it, according to the values shown in Table IV, i.e., by a factor of 0.609 (= 0.719/1.18) to match the corresponding TDM derivative given by the experiment for the ν_3^z component, and by 0.861 (= 0.501/0.582) in order to obtain the same matching in the case of the ν_4^z component. As a result, the modified cross sections (labeled as TDM$^{\text{expt}}$) get in both cases smaller than the ones labeled as TDM$^{\text{calc}}$, and become closer to those given by the dipole Born calculations based on the experimental values. We have also extended this type of sensitivity analysis by modifying the TDM derivative given the calculations by a factor of 1.4. The reason for this scaling will become evident after the following discussion. The resulting cross sections (labeled as TDM$^{\text{scaled}}$) in Figs. 10 and 11 have the height of these peaks near threshold about 1.9 times higher than the ones given by the TDM$^{\text{calc}}$ results. This feature strongly indicates that the inelastic cross sections in the low-energy region of both modes are indeed proportional to the square of the dipole derivative dominating the asymptotic form of the interaction,
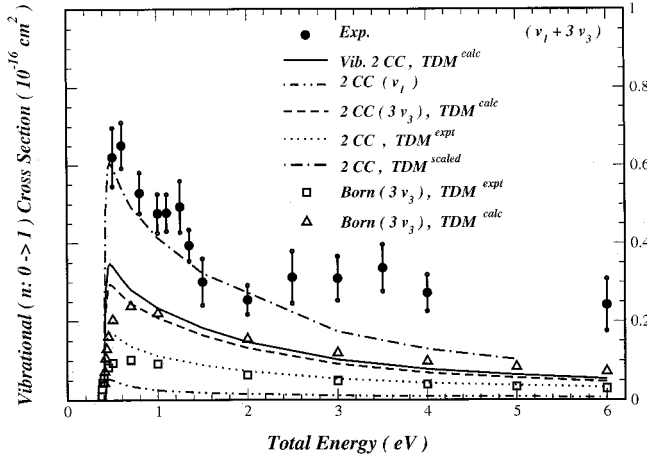
FIG. 12. Vibrational excitation cross sections $(0 \to 1)$ computed with the BF-VCC method for the ν_1 (double dot chain), the $3\nu_3$ (dashed curve), and the weighted sum of the two modes (solid curve). The present calculations are also compared with the experiments [12] for $\nu_1 + 3\nu_3$ modes (filled in circles with error bars). The notation for the other plots is the same as that given in Fig. 10.

as indicated by Eq. (19). Thus, for the ν_3 and the ν_4 modes, our numerical experiments clearly show that the TDM derivative plays an essential role in controlling the size of the inelastic cross sections at low collision energies and therefore will largely control possible agreement with experiments.

We additionally report in Figs. 12 and 13 a comparison between the present calculations and the available experiments [12] for the $(\nu_1 + 3\nu_3)$ and the $(2\nu_2 + 3\nu_4)$ excitation processes, respectively. In Table VI, we also present the numerical values for the vibrational excitation cross sections of all the normal modes obtained in this work via the two-state BF-VCC method. The excitation contributions from the ν_3 and ν_4 modes, given their threefold multiplicities due to the
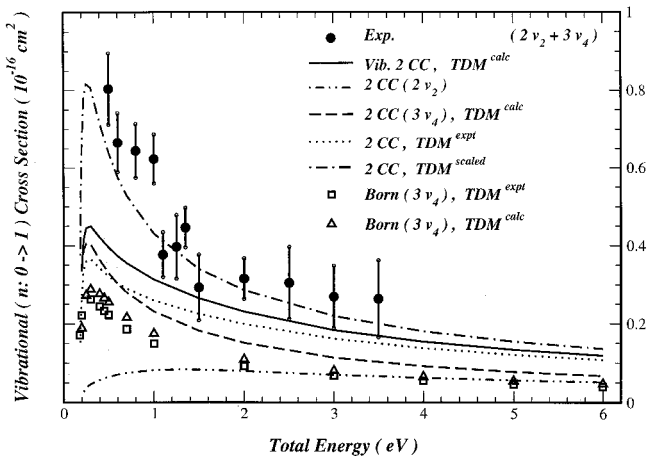

FIG. 13. Same as in Fig. 12 but for the $2\nu_2 + 3\nu_4$ modes. The cross sections reported were computed with the BF-VCC method for the $2\nu_2$ (double dot chain curve), the $3\nu_4$ (dashed curve), and the sum of the two types of modes (solid curve). The notation for the other curves reported is the same as that given in Fig. 11.

TABLE VI. Vibrational excitation cross sections (10^{-17} cm^2) from the two-state BF-VCC calculations for the transition $(0 \to 1)$ of all the CH$_4$ normal modes.

Total energy (eV)	ν_1	$2\nu_2$	$3\nu_3$	$3\nu_4$
0.2				3.350
0.22		0.267		3.878
0.25		0.389		4.058
0.3		0.468		4.031
0.4		0.575		3.636
0.42	0.486		2.244	
0.45	0.529		2.879	
0.47	0.525		2.948	
0.5	0.505	0.652	2.904	3.299
0.6	0.418	0.709	2.663	3.019
0.7	0.351	0.751	2.456	2.800
1.0	0.249	0.818	2.087	2.309
1.5	0.187	0.829	1.641	1.818
2.0	0.153	0.794	1.311	1.510
3.0	0.112	0.701	0.906	1.135
4.0	0.091	0.622	0.686	0.916
5.0	0.078	0.562	0.554	0.774
6.0	0.070	0.516	0.467	0.675

T_2 symmetry, are by far the dominating processes in the inelastic dynamics. From about 2 eV of total energy and all the way up to 6 eV, in fact, we see that the excitation probability of the ν_3 mode is more than five times larger than that of the ν_1, and that of the ν_4 contribution is about two times larger than that from the ν_2. The experimental data for the $(\nu_1 + 3\nu_3)$ are close to the shape produced by our calculations and clearly show the marked increase at threshold of the combined excitation process. The latter is dominated by the transition dipole contribution that is induced by the ν_3 mode and confirms once more the strong effect of such an asymptotic interaction on the low-energy scattering process. On the other hand, the size of our computed cross sections is markedly smaller than the experiments and it becomes remarkably close to them once the TDM contribution is scaled by the factor of 1.4 discussed before.

For the $(2\nu_2 + 3\nu_4)$ our calculations, which implicitly use the computed TDM derivative as shown in Table IV, also turn out to be smaller than the experiments by a factor of nearly 2 although their shape with energy is well reproduced by our results. To test the sensitivity of the computed inelastic contributions by adjusting the TDM derivative for the ν_4 mode, we have artificially scaled the corresponding dipole term by a factor of about 1.4, which corresponds to increasing the experimental TDM value by a factor of 1.63 (see Table IV). We clearly see in Fig. 13 that the scaled inelastic cross sections are now remarkably close to the experimental values, as it occurred with the comparison in Fig. 12.

Finally, we clearly see from the calculations shown in Figs. 12 and 13 that our cross sections computed by employing at threshold scaled TDM values are brought in good agreement with the measured data. Such results indicate, rather interestingly, that positron scattering experiments for

vibrational energy loss processes in polyatomics confirm the dominance of the TDM contribution in controlling the size of the inelastic cross sections near threshold.

IV. PRESENT CONCLUSIONS

The work reported here models at the molecular level the quantum dynamics of vibrational excitation in a nonlinear polyatomic molecule that collides with a beam of low-energy positrons. As far as we are aware, this is the first time that the exact dynamics of the vibrational close-coupling expansion is applied to the real case of a polyatomic target undergoing gas-phase scattering with positron projectiles. We have examined the scattering for all the four normal modes of CH_4 and carried out calculations both at the BF-VCC level of dynamical treatment and with the more approximate ANV convolution procedure. We further tested, for the IR active modes, the validity of the Born calculations by using only the transition dipole interaction in the scattering treatment. Although we are obviously able to compute separately the two stretching (the total symmetric ν_1 and the antisymmetric ν_3) and the two bending (the twisting ν_2 and the scissoring ν_4) contributions, the experiment reveals only two unresolved sets of cross sections for the $(\nu_1 + 3\nu_3)$ and $(2\nu_2 + 3\nu_4)$ modes [12]. Such measurements are, therefore, the final quantities with which we have compared our calculations. The following conclusions could be drawn from our results.

(1) The ν_2 excitation cross sections are smaller than the corresponding ν_4 excitation: the latter process is shown to dominate the overall excitation of CH_4 from an energy of about 0.2 eV up to 6 eV. The result is similar to that for the excitation of the ν_1 mode, which we found to be much smaller than the ν_3 excitation (see also Ref. [16]).

(2) The cross sections for all the modes are found to be rather featureless even close to thresholds and to increase in size as the collision energy decreases. Due to the presence of TDM contributions for the ν_3 and for the ν_4 modes, these two excitations show a more marked increase of their cross sections at threshold, a typical feature also seen in the dipole Born calculations, and in the experimental behavior [12].

(3) The ANV approximation, due to the rather weak nature of the positron coupling with the nuclear motion, appears to hold well for energies away from threshold while, however, exhibiting the wrong energy dependence right at threshold, as already seen in our study of electron/positron-CH_4 vibrational excitation processes [5,6,16].

(4) The present BF-VCC results, and their analysis in terms of different molecular parameters that play a role in the scattering process, provide good physical insight about the details of the vibrational excitation processes at the microscopic level, particularly when we examine the derivatives of the induced dipole moments for the ν_3 and the ν_4 modes and the derivatives of the spherical polarizabilities. The latter were, in fact, found to play a significant role in the ν_1 excitation only, and especially at low collision energies where the long-range interaction dominates the scattering for that mode.

(5) We have further found that discrepancies exist between the values of the TDMs that are obtained from the IR spectroscopy data and the TDM values (expected to dominate the low-energy scattering) that are needed to reproduce the experimentally determined inelastic cross sections. In other words, the experimental cross sections very recently reported [12] seem to be, in the very low energy regions where the values of the induced TDM are thought (and found) to be dominant, larger than the values of cross sections we obtain with our BF-VCC calculations by scaling the employed TDMs to match the IR experiments. In short, our calculations show to be reasonable to use the collisional inelastic cross sections close to threshold to extract estimates for the TDM values, while, at the same time, such estimates appear to be less reliable than those provided by the IR experimental analysis.

(6) Because of the model nature of our chosen interaction, however, the effect of the V^{pcp} contributions in the intermediate and long-range parts of the collisional interaction region cannot be easily evaluated and therefore further computational tests should be carried out to improve agreement with existing experiments. It remains important, however, to have shown with the present study that the ANV dynamical approximations are particularly effective for low-energy positron scattering and that such a simplification will be particularly useful when studying much larger polyatomic gases interacting with positron beams at energies away from the excitation thresholds.

[1] M. Kimura, M. Inokuti, and M. A. Dillon, Adv. Chem. Phys. **84**, 193 (1993).

[2] N. J. Mason, W. M. Johnstone, and P. Akther, in *Electron Collisions with Molecules, Clusters, and Surfaces*, edited by H. Ehrhardt and L. A. Morgan (Plenum, New York, 1994), p. 47.

[3] F. A. Gianturco and T. Mukherjee, Eur. Phys. J. D **7**, 211 (1999); J. Phys. B **30**, 3567 (1997).

[4] F. A. Gianturco and T. Mukherjee, Phys. Rev. A **64**, 024703 (2001); **55**, 1044 (1997).

[5] S. C. Althorpe, F. A. Gianturco, and N. Sanna, J. Phys. B **28**, 4165 (1995).

[6] M. Cascella, R. Curik, and F. A. Gianturco, J. Phys. B **34**, 705 (2001); M. Cascella, R. Curik, F. A. Gianturco, and N. Sanna, J. Chem. Phys. **114**, 1989 (2001).

[7] M. Kimura, O. Sueoka, A. Hamada, and Y. Itikawa, Adv. Chem. Phys. **111**, 537 (2000).

[8] M. Charlton and J. W. Humberston, *Positron Physics* (Cambridge University Press, Cambridge, UK, 2001), p. 40.

[9] D. A. Przybyla, W. E. Kauppila, C. K. Kwan, S. J. Smith, and T. S. Stein, Phys. Rev. A **55**, 4244 (1997).

[10] C. Kurz, S. J. Gilbert, R. G. Greaves, and C. M. Surko, Nucl. Instrum. Methods Phys. Res. B **143**, 188 (1998).

[11] J. P. Sullivan, S. J. Gilbert, and C. M. Surko, Phys. Rev. Lett. **86**, 1494 (2001).

[12] J. P. Sullivan, S. J. Gilbert, J. P. Marler, L. D. Barnes, S. J. Buckman, and C. M. Surko, Nucl. Instrum. Methods Phys. Res. B (to be published).

[13] F. A. Gianturco, T. Mukherjee, and P. Paioletti, Phys. Rev. A **56**, 3638 (1997).

[14] Y. Itikawa, Int. Rev. Phys. Chem. **16**, 155 (1997).

[15] N. Chandra and A. Temkin, Phys. Rev. A **13**, 188 (1976).

[16] T. Nishimura and F. A. Gianturco, Nucl. Instrum. Methods Phys. Res. B **192**, 17 (2002).

[17] F. A. Gianturco, T. Mukherjee, T. Nishimura, and A. Occhigrossi, in *New Directions in Antimatter Chemistry and Physics*, edited by C. M. Surko and F. A. Gianturco (Kluwer, Dordrecht, 2001), p. 451.

[18] P. G. Burke, N. Chandra, and F. A. Gianturco, J. Phys. B **5**, 2212 (1972).

[19] E. Boronski and R. M. Nieminen, Phys. Rev. B **34**, 3820 (1986).

[20] W. Kohn and L. J. Sham, Phys. Rev. **137**, A1697 (1965); **140**, A1133 (1965).

[21] A. Jain and F. A. Gianturco, J. Phys. B **24**, 2387 (1991).

[22] T. Nishimura and Y. Itikawa, J. Phys. B **28**, 1995 (1995); **29**, 4213 (1996).

[23] H. T. Davis and L. D. Schmidt, Chem. Phys. Lett. **16**, 260 (1972).

[24] E.g., F. A. Gianturco, D. G. Thompson, and A. Jain, in *Computational Methods for Electron-Molecule Collisions*, edited by W. M. Huo and F. A. Gianturco (Plenum, New York, 1995), p. 75; F. A. Gianturco and A. Jain, Phys. Rep. **143**, 347 (1986).

[25] M. J. Frish *et al.*, GAUSSIAN 98, Revision A.7 (Gaussian, Pittsburgh, PA, 1998).

[26] T. N. Rescigno and A. E. Orel, Phys. Rev. A **24**, 1267 (1981); **25**, 2402 (1982).

[27] D. E. Woon and T. H. Dunning Jr., J. Chem. Phys. **98**, 1358 (1993).

[28] D. J. Swanton, G. B. Bacskay, and N. S. Hush, J. Chem. Phys. **84**, 5715 (1986).

[29] D. M. Bishop and L. M. Cheung, J. Phys. Chem. Ref. Data **11**, 119 (1982).

[30] O. Sueoka and S. Mori, J. Phys. B **19**, 4035 (1986).

[31] T. Nishimura and F. A. Gianturco, J. Phys. B (to be published).

[32] T. Shimanouchi, in *Tables of Molecular Vibrational Frequencies Consolidated*, Natl. Bur. Stand. Ref. Data Ser., Natl. Bur. Stand. (U.S.), No. 39 (US GPO, Washington, DC, 1972), Vol. 1, p. 45.